Int J Adv Manuf Technol (2017) 91:1275–1287
DOI 10.1007/s00170-016-9790-y

ORIGINAL ARTICLE

Influence of die geometric structure on flow balance in complex hollow plastic profile extrusion

Yue Mu [1,2] · Lianqiang Hang [1,2] · Anbiao Chen [2] · Guoqun Zhao [1,2] · Dingding Xu [3]

Received: 26 June 2016 / Accepted: 18 November 2016 / Published online: 3 December 2016

Abstract The unbalanced flow problem often occurs at die exit in the extrusion process of plastic profile, which directly influences the performance of final products. For the lack of corresponding theoretical basis, reasonable extrusion die design is still a difficult task, especially for the complex hollow profile. With the development of computational fluid dynamics theory, numerical method becomes an effective way to investigate the complex material forming problems. In the present study, a design strategy for complex hollow profile extrusion die was proposed based on the principles of flow balance. The mathematical model for three-dimensional non-isothermal polymer melt flow within complex extrusion die runner was developed based on the computational fluid dynamics (CFD) theory. The governing equations were deduced based on the finite volume method, and the pressure-velocity coupling problem was solved by using the Semi-Implicit Method for Pressure-Linked Equations (SIMPLE) algorithm. The Arrhenius equation was employed to involve the temperature dependence of material parameters. The flow characteristics of PVC polymer melts in the extrusion process of complex hollow profile were investigated. The distributions of principal field variables including flow velocity, melt temperature, and pressure drop were obtained. The effects of die geometric parameters on the velocity distribution uniformity were further analyzed, and a design strategy was proposed to achieve the flow balance in complex plastic profile extrusion process.

Keywords Profile extrusion · Die design · Finite volume simulation · Flow balance

✉ Yue Mu
ymu@sdu.edu.cn

✉ Guoqun Zhao
Zhaogq@sdu.edu.cn

[1] Key Laboratory for Liquid-Solid Structural Evolution and Processing of Materials, Ministry of Education, Shandong University, Jinan, Shandong 250061, People's Republic of China

[2] Engineering Research Center for Mould & Die Technologies, Shandong University, Jinan, Shandong 250061, People's Republic of China

[3] Ningbo Institute of Industrial Technology, Chinese Academy of Sciences, Ningbo, Zhejiang 315201, People's Republic of China

1 Introduction

The complex hollow plastic profile is widely used in the automobile, traffic, construction, and other industries for its delicate structure and diverse function. Unlike common extrusion products, the hollow profile has complex cross section and large variations of wall thickness. The control of flow balance at the die exit in complex hollow profile extrusion process is rather difficult [1, 2]. The manufacturing of profiles with complex structure still now depends on operating experiences derived from many times of trial-and-error method [3]. Traditional experimental method is difficult to be directly conducted in such complex processing operations [4]. Hence, numerical method becomes an effective way to aid the die design in complex hollow plastic profile extrusion, which saves lots of resource and meanwhile improve the product quality.

Many researches have been devoted to investigating rational design strategy of the flow channel and die structure in complex hollow plastic profile extrusion. The cross-sectional method was used for the design and optimization of complex profile extrusion die, where 2D slices perpendicular to the die axis were extracted through the flow channel [5, 6]. Ettinger

[7] employed the cross-sectional method coupled with different optimization methods like global optimization scheme, sequential optimization scheme, height approximation method, and parallel decoupled scheme for the automated design of uPVC profile extrusion dies. Mu [8] proposed an optimization strategy for the die design in polymer extrusion process based on finite element simulation, back-propagation neural network, and non-dominated sorting genetic algorithm II, which was successfully applied to LDPE annular extrusion process. Yilmaz [9] adopted several objective functions defined by simulated annealing-kriging meta-algorithm to optimize the geometric parameters of a simple-shape profile extrusion die. In order to achieve balanced flow at the die exit, a design of flow separator was proposed to prevent cross flows [10, 11]. However, the addition of flow separator may have negative effect on mechanical properties of the produced profile due to possible welding lines at the interface of subsections [12, 13]. Hence, comprehensive understanding of material forming mechanism within the flow channel is the foundation of rational extrusion die design. In practical processing, polymer melt flow within the extrusion die runner can be considered as non-isothermal incompressible non-Newtonian fluid. A number of numerical methods have been developed to investigate the flow and heat transfer problem in polymer processing, including the finite difference method (FDM) [14], the finite element method (FEM) [15, 16], the finite volume method (FVM) [17, 18], the pseudo-spectral method [19], and the boundary element method [20, 21], which help to understand the mechanism of extrudate swell, wall slip, and other unique forming phenomenon. Among these methods, the FVM based on the Euler description is widely used for its adaptability to complex geometries that avoids re-meshing and its better maintenance of conservation of original governing equations.

As for the hollow plastic profile with complex structure, the achievement of balanced flow at die exit is a major task in the design of extrusion die. In the study, the design strategy for complex hollow profile extrusion die was investigated based on the principle of flow balance. The modeling for three-dimensional non-isothermal polymer melt flow within complex extrusion die runner was presented. The discretization of governing equations was deduced based on the FVM, and the Semi-Implicit Method for Pressure-Linked Equations (SIMPLE) algorithm was adopted to solve the pressure-velocity coupling problem. The flow characteristics of polymer melts in the die runner of complex hollow profile extrusion were investigated based on the developed numerical algorithm. The influence of die geometric parameters including the flow channel structure of inner ribs and functional block regions on the uniformity of velocity distribution at the die exit was further analyzed. Reasonable advice on the design of the extrusion die runner was accordingly put forward for the forming of complex hollow plastic profile.

2 Design strategy of extrusion die runner

In the extrusion process of plastic profile, the extrusion die contributes in three aspects including flow stabilization, flow division, and shaping for the plastic profile. The design strategy of extrusion die runner needs to ensure the equivalence of the average velocity for each part of profile cross section at exit of die lip. Otherwise, the shape of various parts after leaving the die exit will change differently under the same pulling speed, and the part where velocity is large will experience volume increase than the part having small velocity, which directly influences shape and dimension precision of the final products.

The die design strategy for a commercially applied hollow plastic profile with the cross-sectional structure as shown in Fig. 1a is investigated in the study. Considering the comprehensive effects of extrusion swelling, cooling shrinkage, and drawing shrinkage, the extrusion die lip is designed as shown in Fig. 1b. According to the difference of function and location, the structure of plastic profile can be divided into three

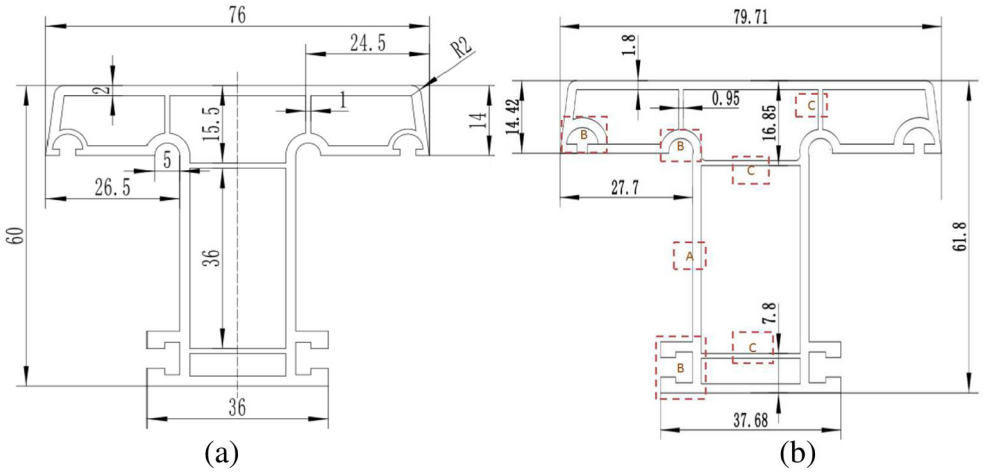

Fig. 1 Cross-sectional geometric parameters: **a** profile and **b** die lip

parts including the mainframe region (A), the functional block region (B), and the inner rib region (C). For the reason of large variation in wall thickness of the hollow plastic profile, a design strategy that separates the outer and the inner flow channels is adopted in the study. Where, the outer flow channel is used to form the mainframe region (A) and the functional block region (B), the inner flow channel is used to form the inner rib region (C). Considering the complex structure and shape transition within the die runner, a ray-tracing and proportional-spacing hybrid approach is applied in the design of outer flow channel to avoid abrupt shape transition and reduce the effects of elastic recovery [22].

A streamline extrusion die runner is designed as shown in Fig. 2, which consists of an expansion section L_1, an adapter section L_2, a transition section L_3, and a parallel section L_4. The shape transition of cross section along flow direction within the die runner is shown in Fig. 3. In the expansion section, the transition from the circular die inlet to the adapter is gently realized to avoid abrupt transverse flow, where the expansion angle is controlled to be less than 30°. In order to control the compression ratio that is defined to be the ratio of cross-sectional area of adapter section to the parallel section, the outer dimension of the adapter section is obtained by extending the boundary of the parallel section outward about 0.004 m. The transition of adapter section to the parallel section is realized through reasonable design of the transition section. According to the restriction on the contraction angle that belongs to 10°–20°, the length of the transition section is defined to be 0.02 m. In the parallel section, simple shearing flow makes macromolecular chain relax to a certain extent, which can reduce the effects of flow history derived from complex cross-sectional transition within the die runner. The length of the parallel section is experientially taken as $L_4 = (20 - 50)h$, where h is the gap height of the die lip.

It is difficult to directly determine whether the current designed die runner can achieve balanced flow. The evaluation of die geometric effect on the flow balance is hence performed based on numerical analysis of the flow characteristics within complex flow channel as discussed in the following sections.

3 Modeling of polymer flow within die runner

3.1 Governing equations

According to the computational fluid dynamics (CFD) theory, the governing equations can be obtained according to the conservation of mass, momentum, and energy. Considering the practical flow state, polymer melts within die runner can be seen as incompressible non-Newtonian fluid. Due to high viscosity of the polymer melts, the volume force and surface force can be ignored relative to the viscous shear force. The flow is regarded as steady laminar for relatively low Reynolds number. The governing equations for the polymer melt flow can hence be simplified as follows:

$$\text{Continuity equation} \quad \nabla \cdot \boldsymbol{U} = 0 \tag{1}$$

where $\boldsymbol{U}$ is the velocity vector and ∇ is the Hamilton differential operator.

$$\text{Momentum equation} \quad \nabla \cdot (\rho \boldsymbol{U}\boldsymbol{U}) = \nabla \cdot \boldsymbol{\sigma} \tag{2}$$

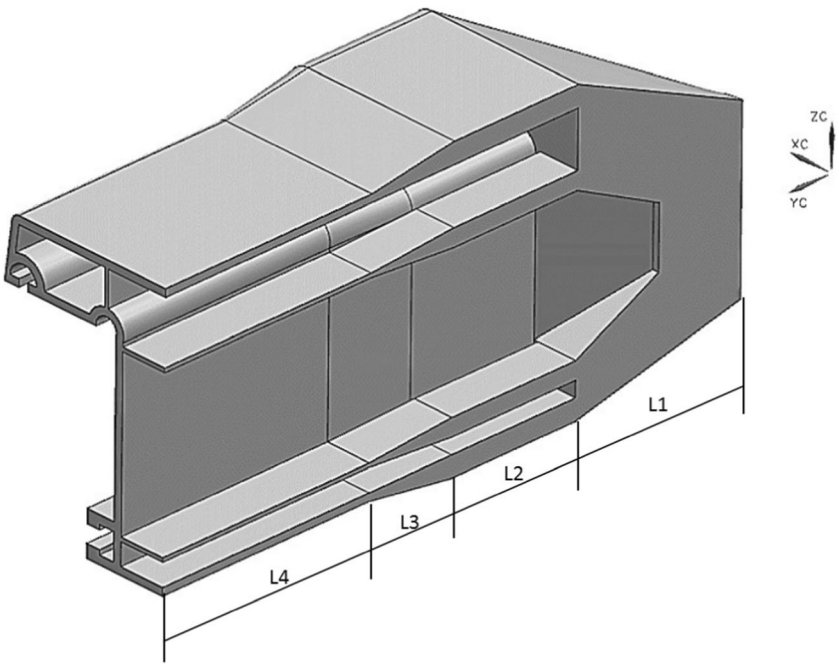

Fig. 2 Geometrical structure of the extrusion die runner

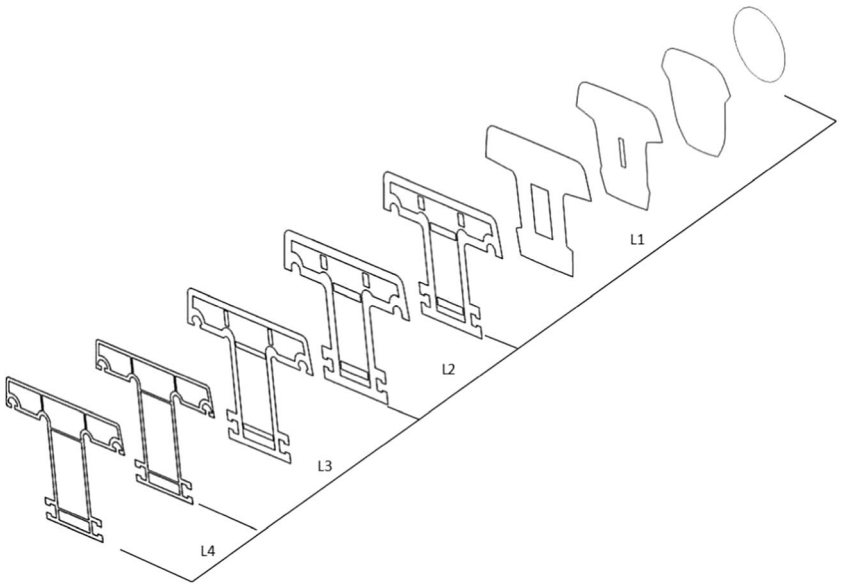

Fig. 3 Cross-sectional shape transition within the die runner

where ρ is the density and $\boldsymbol{\sigma}$ is the Cauchy stress tensor, which can be expressed as

$$\boldsymbol{\sigma} = -P\boldsymbol{I} + \boldsymbol{\tau} \tag{3}$$

where $\boldsymbol{P}$ is the hydrostatic pressure, $\boldsymbol{I}$ is the Kronecker delta, and $\boldsymbol{\tau}$ is the extra stress tensor that obeys the following relationship for viscous fluid:

$$\boldsymbol{\tau} = 2\eta\boldsymbol{d} \tag{4}$$

where η is the apparent viscosity and $\boldsymbol{d} = (\nabla\boldsymbol{U} + \nabla^T\boldsymbol{U})/2$ is the strain rate tensor.

$$\text{Energy equation} \quad \rho C_P \nabla\cdot(T\boldsymbol{U}) = -\nabla\cdot q + Q \tag{5}$$

where C_P is the heat capacity, T is the temperature, q is the heat flux, and Q is the total source term. The heat flux Fourier's law of heat conduction is assumed with an isotropic thermal conductivity $q = -k\nabla T$ for the steady flow, where k is the thermal conductivity. The polymer melt flow in the die runner is regarded as viscous flow, and all the mechanical energy is assumed to be dissipated as heat, and the total source term equals to viscous heat dissipation $Q = \boldsymbol{\tau} : \boldsymbol{d}$.

3.2 Material model

Considering the flow characteristics of polyvinyl chloride (PVC) within the extrusion die runner, the material viscosity is the function of shear rate γ that obeys the Bird-Carreau model

$$\eta = \eta_\infty + (\eta_0 - \eta_\infty)\left[1 + (\lambda\gamma)^2\right]^{(n-1)/2} \tag{6}$$

$$\gamma = \sqrt{2\boldsymbol{d}(\boldsymbol{U}) : \boldsymbol{d}(\boldsymbol{U})} \tag{7}$$

where η_0 is the zero shear viscosity, η_∞ is the infinite shear viscosity, λ is the relaxation time, and n is the flow index.

The coupling between the momentum and energy conservation equations is achieved through temperature-dependent material viscosity as the following Arrhenius equation:

$$\eta_0(T) = \eta_0(T_0)\exp\left[\frac{\Delta E}{R}\left(\frac{1}{T} - \frac{1}{T_0}\right)\right] \tag{8}$$

where $\eta_0(T_0)$ denotes the value of zero shear viscosity at reference temperature T_0, ΔE is the activation energy, and R is the universal gas constant.

The corresponding material parameters of PVC melt flow within the extrusion die runner are listed in Table 1.

3.3 Mesh division

Considering the demands on calculation accuracy and the adaptability to complicated geometric structure of the extrusion die runner, a hybrid meshing division is adopted for the spatial discretization. As it is shown in Fig. 4, the flow domain within the die runner is divided into 6,250,000 brick elements. The adapter section and the parallel section are divided using hexahedral grid, while the expansion section and the transition

Table 1 Material parameters

Parameter	Value
ρ(kgm^{-3})	1400
C_P(Jkg^{-1}K^{-1})	1400
k(Wm^{-1}K^{-1})	0.14
η_0(Pa s)	10,000
η_∞(Pa s)	500
λ(s)	0.6
n	0.29

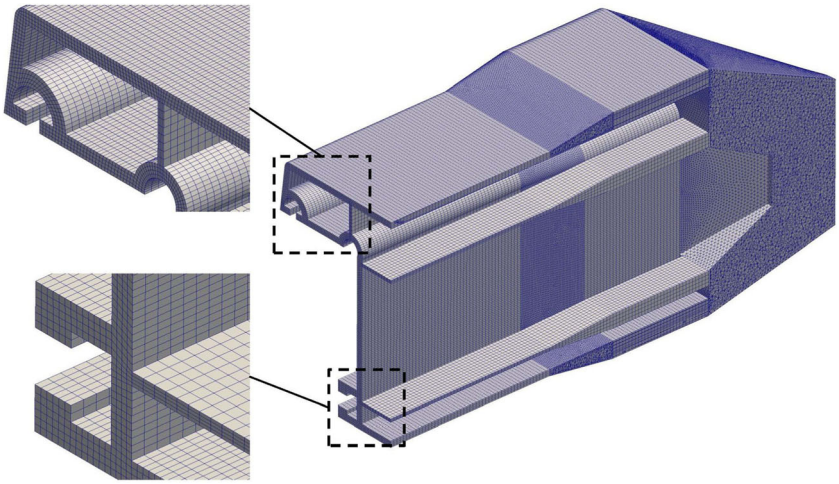

Fig. 4 Mesh division of the flow channel

section are divided using tetrahedral grid. The FVM is adopted for discretization of the governing equations based on the hybrid meshing division strategy, which will be detailedly discussed in the following sections.

3.4 Boundary conditions

Boundary conditions are required for the dependent variables at boundary faces of the computational domain in the finite volume simulation. Considering the practical flow characteristics in the profile extrusion process, the velocity that is normal to the inlet of die runner is taken as $u_{\text{inlet}}=0.1\text{m/s}$ and a fixed melt temperature $T_{\text{inlet}}=453\text{K}$ is imposed on the inlet face of the die runner. On the outlet cross section, the values of the relative pressure and the streamwise gradient for temperature are set to be zero. On the solid die wall, the non-slip condition is imposed. The velocity components of polymer melts contacted to the die wall are set to be $u_X=u_Y=u_Z=0$. An adiabatic contact is imposed on the solid die wall, and the temperature rise of polymer melts in the die runner is due to viscous heat dissipation with ignoring outer thermal conductivity. By substituting $u_X=u_Y=u_Z=0$ into the momentum equation, the approximation of pressure boundary on the die wall $\nabla P=0$ can be obtained.

4 Numerical algorithm

4.1 Discretization of the governing equations

The common form of the governing equations Eq.(1), Eq.(2), and Eq.(5) can be written as Eq.(9) by introducing the general tensor φ

$$\nabla\cdot(\rho\boldsymbol{U}\varphi)-\nabla\cdot(\Gamma\nabla\varphi)=S(\varphi) \tag{9}$$

After being integrated within the control volume P, the following equation can be obtained:

$$\int_{V_P}\nabla\cdot(\rho\boldsymbol{U}\varphi)-\int_{V_P}\nabla\cdot(\Gamma\nabla\varphi)dV=\int_{V_P}S(\varphi)dV \tag{10}$$

According to the Gauss divergence theorem, the body integral form can be converted into the area integral form as follows:

$$\int_{V_P}\nabla\cdot(\rho\boldsymbol{U}\varphi)dV=\int_{S}dS\cdot(\rho\boldsymbol{U}\varphi)=\sum_{f}S\cdot(\rho\boldsymbol{U})_f\varphi_f \tag{11}$$

$$\int_{V_P}\nabla\cdot(\Gamma\nabla\varphi)\,dV=\int_{S}dS\cdot(\Gamma\nabla\varphi)=\sum_{f}(\Gamma)_fS\cdot(\nabla\varphi)_f \tag{12}$$

where φ_f is the value of the variable φ in the center of cell surface f.

The discrete form of governing equations can hence be obtained as follows:

$$\text{Continuity equation}\quad\int_{V_P}\nabla\cdot\boldsymbol{U}dV=\sum_{f}S\cdot\boldsymbol{U}_f=0 \tag{13}$$

$$\text{Momentum equation}\quad\sum_{f}S\cdot(\rho\boldsymbol{U})_f\boldsymbol{U}_f-\sum_{f}\eta S\cdot(\nabla\boldsymbol{U})_f=-V_P\nabla P \tag{14}$$

$$\text{Energy equation}\quad C_P\sum_{f}S\cdot(\rho\boldsymbol{U})_fT_f-\sum_{f}kS\cdot(\nabla T)_f=\eta\dot{\gamma}^2V_P \tag{15}$$

After spatial discretization, the governing equations in each control volume can be written as the following algebraic equation:

$$a_P\varphi_P+\sum_{N}a_N\varphi_N=R_P \tag{16}$$

where φ_N is the value of the variable φ in the adjacent control volume N.

The global stiffness matrix equation of the governing equations for all the control volume within the calculation domain can be assembled as

$$\boldsymbol{A\Phi} = \boldsymbol{R} \tag{17}$$

where $\boldsymbol{A}$ is the global stiffness matrix, $\boldsymbol{\Phi}$ is the component of all variables, and $\boldsymbol{R}$ corresponds to the equation source items.

The ICCG and Bi-CGSTAB iterative solution is adopted in the calculation of above large non-linear algebraic equations [23, 24]. The relaxation factor κ is introduced in each control volume to avoid the computational divergence as follows:

$$\varphi_P^i = \varphi_P^{i-1} + \kappa\left(\frac{R_P - \sum_N a_N\varphi_N^i}{a_P} - \varphi_P^{i-1}\right) \tag{18}$$

The following iterative equation can hence be obtained:

$$\frac{a_P}{\kappa}\varphi_P^i + \sum_N a_N\varphi_N^i = R_P + \frac{1-\kappa}{\kappa}a_P\varphi_P^{i-1} \tag{19}$$

where i is the current iterative step and $i-1$ is the last iterative step.

The convergence criteria are defined upon the requirements on velocity, pressure, and temperature fields. When the relative error of each variable is less than a set value, convergence is considered to be achieved. Based on the converged fundamental solution, the viscosity, stress tensor, and strain rate tensor can be derived.

4.2 Pressure-velocity decoupling calculation

In the governing equations, the pressure and velocity are coupled together and the pressure gradient is part of the source term in the momentum equation. In order to avoid oscillations in pressure solution, the SIMPLE algorithm is adopted in the study [25]. According to the discrete form of the momentum equation, the following semi-discrete equation can be obtained:

$$a_P U_P = H(U)_P - (\nabla P)_P \tag{20}$$

where $H(\boldsymbol{U})_P = \sum_N a_N \boldsymbol{U}_N$.

The initial pressure field is firstly assumed to be P^*. After substituting P^* into the semi-discrete momentum equation Eq. (20), the velocity field $\boldsymbol{U}^*$ can be obtained. However, the velocity field $\boldsymbol{U}^*$ calculated based on P^* is always difficult to satisfy mass conservation. A velocity correction term $\boldsymbol{U}' = \boldsymbol{U} - \boldsymbol{U}^*$ and a pressure correction term $P' = P - P^*$ that satisfy $\boldsymbol{U}' = -\frac{1}{a_P}\left(\nabla P'\right)_P$ are hence introduced, and the following velocity correction equation can be obtained:

$$\boldsymbol{U} = \boldsymbol{U}^* - \frac{1}{a_P}\left(\nabla P'\right)_P \tag{21}$$

After substituting the corrected velocity field $\boldsymbol{U}$ into the mass conservation equation, the pressure correction equation can be obtained:

$$\frac{1}{a_P}\left(\nabla P'\right)_P = \nabla\cdot\boldsymbol{U}^* \tag{22}$$

According to the velocity field calculated through previous iteration, the pressure correction value all over the calculated domain can be obtained through Eq. (22). After substituting the pressure correction value into Eq. (21), the corrected velocity field $\boldsymbol{U}$ can hence be obtained.

5 Results and discussion

Based on the established numerical model and solution algorithm, the essential flow characteristics of polymer melts within the die runner in complex hollow plastic profile extrusion process are successfully predicted and the influence of die geometric structure on the flow balance is further investigated.

5.1 Flow characteristics within die runner

Owing to complex structure of the extrusion die runner, polymer melts experience different flow resistances along the flow path, which causes the variations of flow velocity, pressure drop, and melt temperature. The flow balance can be evaluated through the investigation of flow velocity distribution within the die runner and hence to provide design strategy for the die runner. Figure 5 shows the whole distribution tendency of axial flow velocity U_Y on different cross sections. It can be found that the value of axial flow velocity decreases rapidly in the expansion section (zone 1) as shown in Fig. 5b, c. The newly oriented flow is developed in the adapter (zone 2) as shown in Fig. 5d, e, where the velocity difference between the inner flow channel for inner rib region and the outer flow channel for mainframe and functional block regions is found to increase with the structure variation of die runner. The melt flow is then converted to the required shape and dimension through the contraction in the transition section. The preliminarily formed polymer melts enter the parallel section (zone 3), and a relatively lager velocity gradient occurs as shown in Fig. 5f, g. It is a key

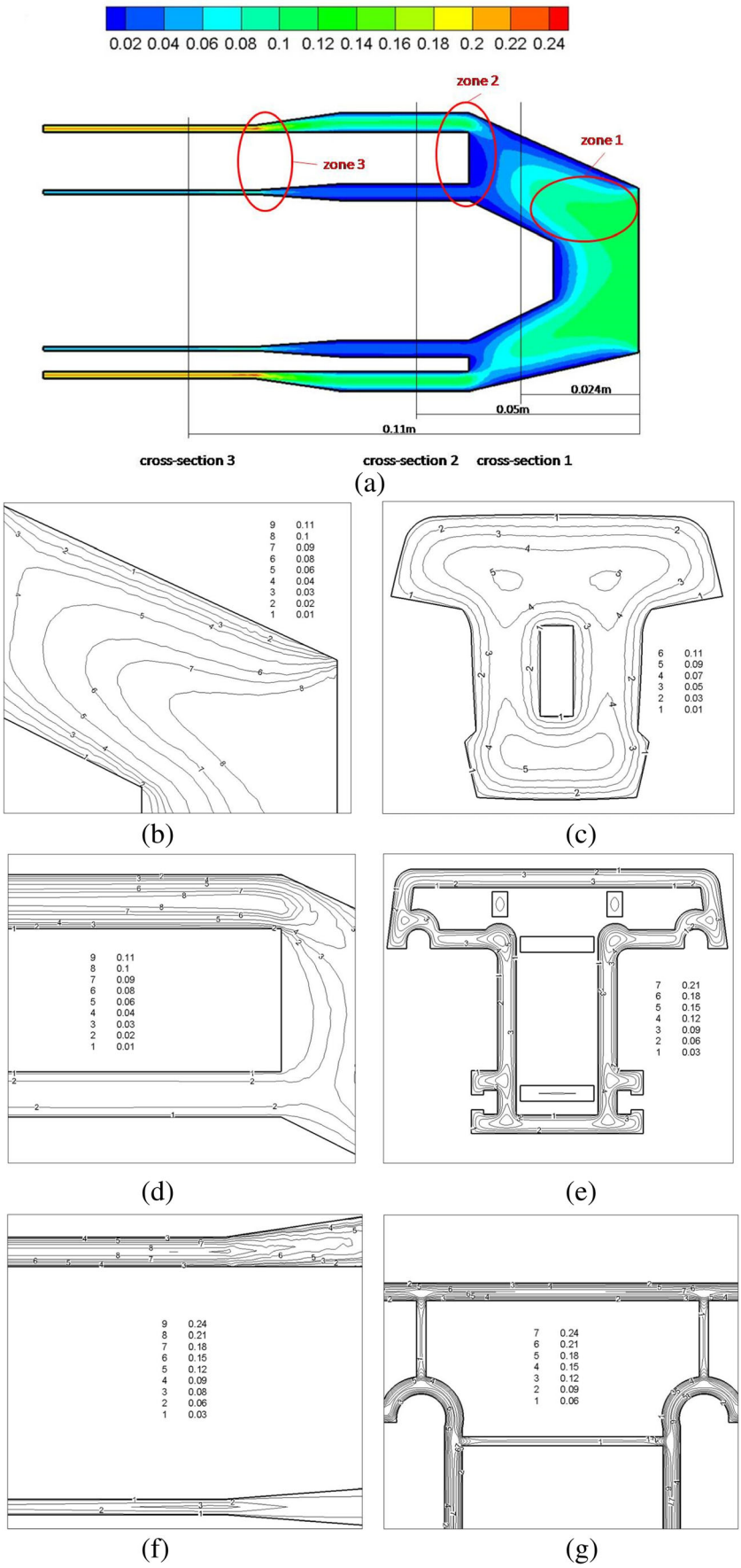

Fig. 5 Distribution of axial flow velocity U_Y(m/s): **a** contours of axial flow velocity U_Y on the $x = 0$ cross section, **b** contours of axial flow velocity U_Y in zone 1, **c** contours of axial flow velocity U_Y on cross section 1, **d** contours of axial flow velocity U_Y in zone 2, **e** contours of axial flow velocity U_Y on cross section 2, **f** contours of axial flow velocity U_Y in zone 3, and **g** contours of axial flow velocity U_Y on cross section 3

factor for successful die design in the polymer extrusion process to achieve uniform flow distribution on the cross section of die lip, which is usually called the flow balance principle. Figure 6 shows the distribution of axial velocity U_Y at the die lip. It can be found that axial flow velocities in the mainframe and functional block regions are relatively larger than those in the inner rib regions. This is owing to the difference of flow resistance when polymer melts flow along different journeys in the die runner. Hence, in order to achieve flow balance, some modifications have to be made to current structure of die runner, which will be detailedly discussed in the next section. Pressure drop of polymer melts within the die runner is also an important parameter from which we can assess energy assumption during the extrusion process. Figure 7 shows the pressure distribution within the die runner. It can be found that the transition section and the parallel section occupy main pressure loss, which is in accordance with the distribution of velocity field. As a result of complex structure variation of the die runner, polymer melts experience strong shear and deformation, which lead to locally viscous heat dissipation, and the change of temperature distribution correspondingly occurs. This will influence the distribution of viscosity in the die runner. High temperature may cause melt degradation or earlier crosslink of the polymer

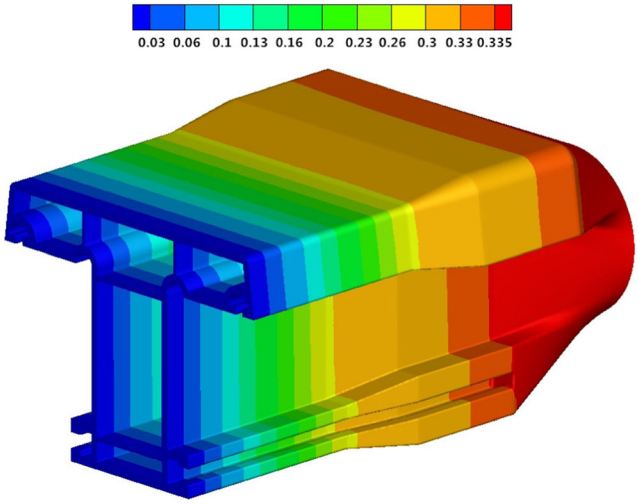

Fig. 7 Pressure distribution within the flow channel (MPa)

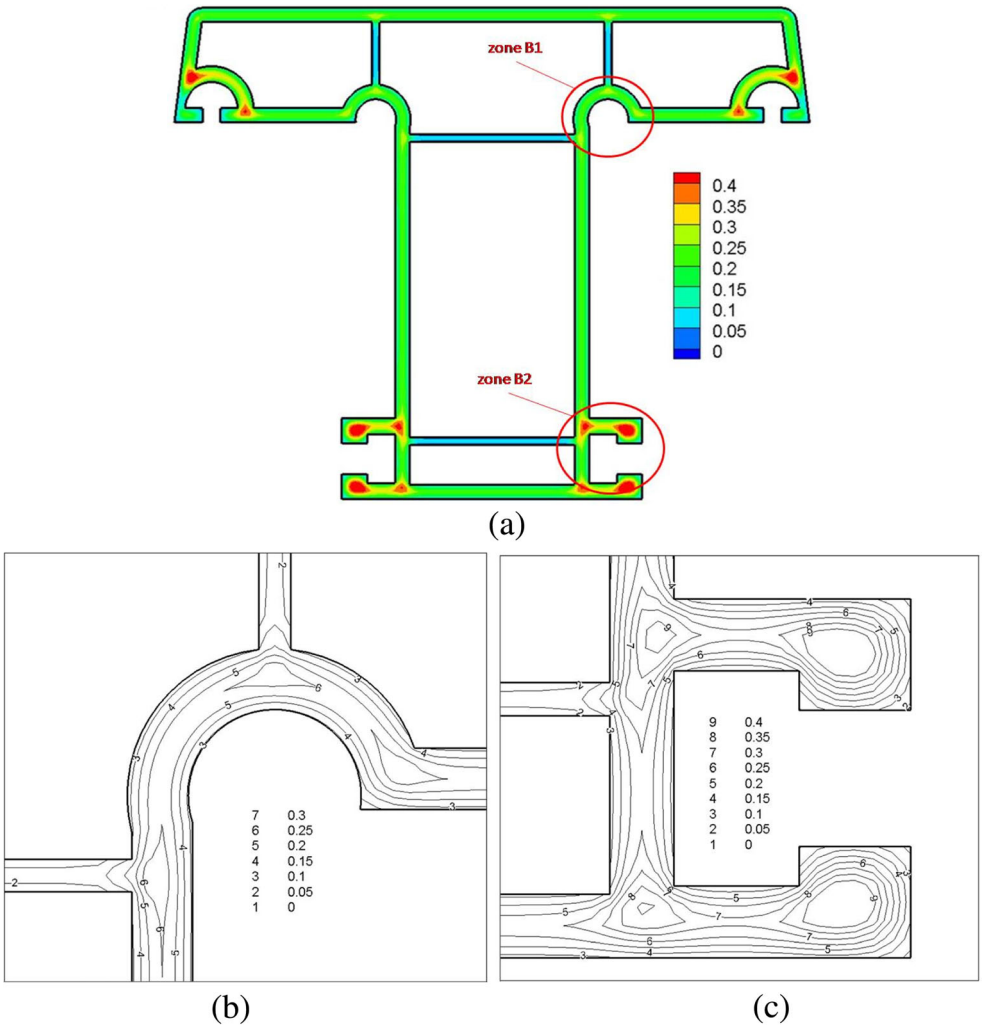

Fig. 6 Contours of axial flow velocity U_Y (m/s): **a** contours of axial flow velocity U_Y on the cross section of die lip, **b** contours of axial flow velocity U_Y in functional block region B1, and **c** contours of axial flow velocity U_Y in functional block region B2

melts, especially for those thermal-sensitive materials. Therefore, good prediction of thermal effect is of much importance to the property of final products. As it is shown in Fig. 8, polymer melts are subject to much stronger shear effect near the die wall where temperature obviously increases and relative low temperature occurs in the center of flow channel where polymer melts experience weaker shear effect. Hence, the viscosity of the polymer melts contacting with the die wall tends to be decreased, and it is the sensitive part where flow instability is likely to occur and should be well controlled. Besides, it can also be found that the maximum temperature occurs around the corner points on functional block regions where polymer melts suffer larger velocity gradient.

5.2 Die geometric effects on flow balance

The achievement of balanced flow is one of the major principles in the die design of plastic profile extrusion. Uniform distribution of flow rate can reduce the residual stress of final products and so as to prevent quality defect like distortion. Velocity distribution at the die lip is related to the flow resistance that polymer melts experienced in the die runner. It can be adjusted by modifying the parameters of die/mould. As for the hollow plastic profile as shown in Fig. 1, flow balance is difficult to be controlled because of complex structure variations between the mainframe region A, functional block region B, and inner rib region C. Based on the numerical investigation of polymer melt flow within the die runner, the effects of die geometric parameters on the flow balance are investigated and reasonable die design strategy is accordingly proposed. In this study, the balance of flow velocity distribution is evaluated by using the velocity relative difference δU on the outlet cross section, which is defined as

$$\delta U = \frac{\sum_{i=1}^{m} \frac{\left|U_i - \overline{U}\right|}{\overline{U}}}{m} \times 100\% \tag{23}$$

where U_i is the flow velocity at each node on the outlet cross section, $\overline{U}$ is the mean flow velocity at the die exit, and m is the total number of nodes on the outlet cross section.

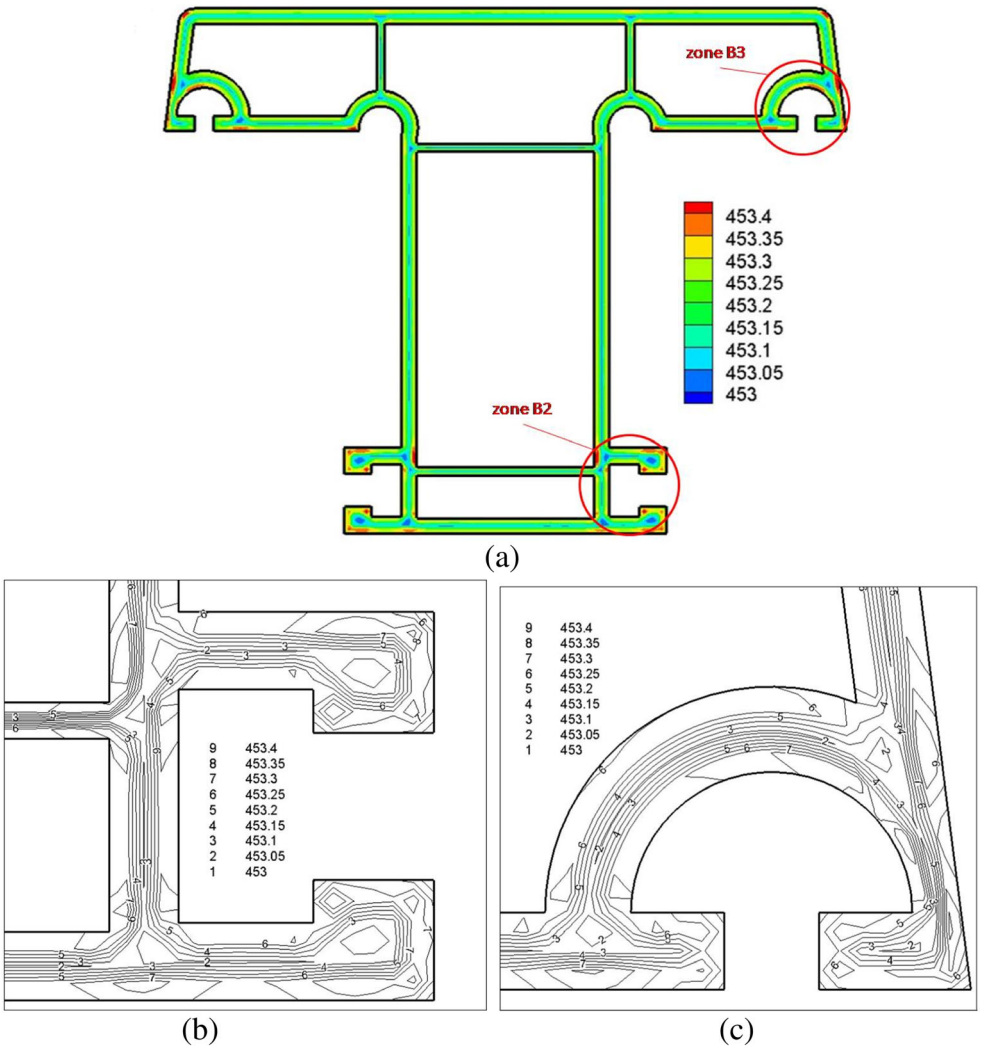

Fig. 8 Temperature distribution (K): **a** contours of temperature on the cross section of die lip, **b** contours of temperature in functional block region B2, and **c** contours of temperature in functional block region B3

According to the numerical results of flow characteristics within current designed die runner, the melt flow within inner rib regions is obviously slower than that within the other regions as shown in Fig. 5. To achieve equivalence of outlet velocity for the inner rib regions and the mainframe regions, the length of the parallel section L and the gap height of adapter section t of the inner flow channel in inner rib region as shown in Fig. 9 are considered to be adjusted in the study. Five structures of inner flow channel with different parallel section lengths L(L = 0.05,L = 0.04, L = 0.03,L = 0.02,L = 0.01 m) are employed to investigate the effects of parallel section length on the flow balance. Figure 10 shows the velocity relative difference δU on the flow channel outlet and the maximum pressure drop ΔP versus different parallel section lengths. It can be found that the velocity relative difference on the outlet cross section decreases with the decrease of the parallel section length of the inner flow channel. That is to say, the melt flow can be well redistributed at the die exit if the length of the parallel section in the inner rib region is designed to be smaller, and the melt flow in the inner rib regions can be better integrated with that in the mainframe regions. With the decrease of velocity relative difference δU, the pressure drop decreases slightly, which may reduce the extrusion power to some extent. Another important design parameter is the compression ratio, which can be defined as the area ratio of the adapter cross section to the parallel cross section. In the study, the compression ratio is adjusted by modifying the gap height of the adapter section within the flow channel of inner rib regions. Based on the parallel section length L = 0.01 m, five structures of inner flow channel with different compression ratios are employed to investigate the effects of gap height

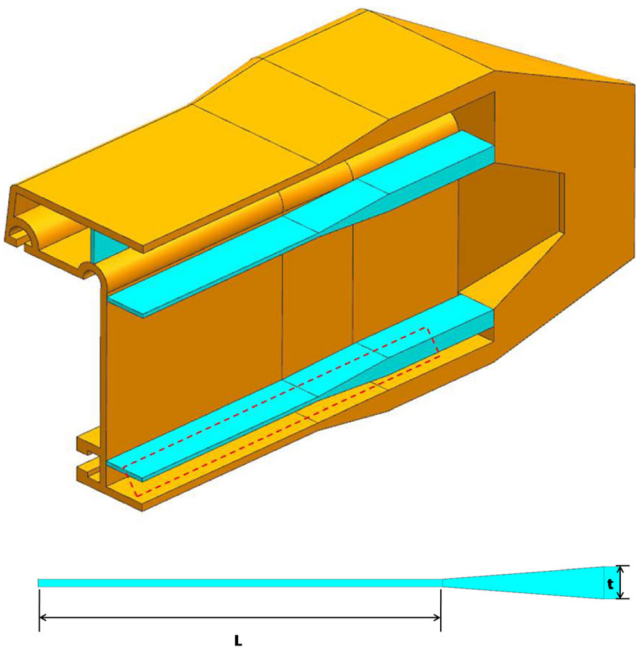

Fig. 9 Geometric parameters of the inner flow channel in inner rib region

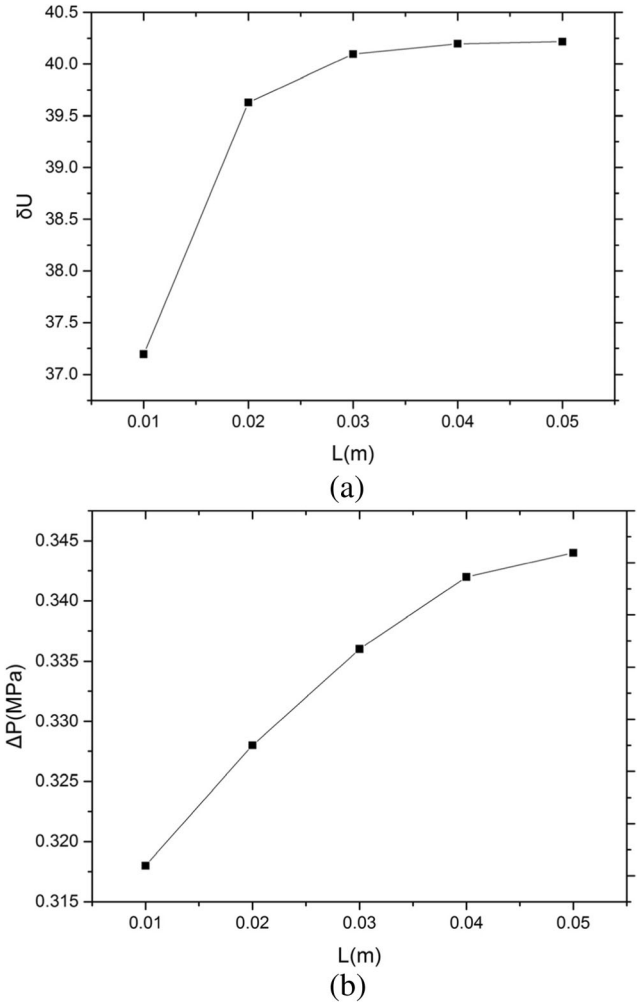

Fig. 10 Variation of flow balance versus different parallel section lengths: **a** velocity relative difference δU and **b** maximum pressure drop ΔP

t(t = 0.003, t = 0.004, t = 0.005, t = 0.006, t = 0.007 m) on the flow balance. Figure 11 shows the velocity relative difference δU on the flow channel outlet and the maximum pressure drop ΔP versus different compression ratios. It can be found that the velocity relative difference δU on the outlet cross section and the maximum pressure drop ΔP decrease with the increase of compression ratio. Therefore, to reduce the length of the parallel section L and to increase the gap height of adapter section t of the inner flow channel in inner rib regions are an effective way to achieve flow balance.

According to the numerical results of flow characteristics within current designed die runner as shown in Fig. 6, we can also find that the melt flow in the corner and intersection of the functional block regions is obviously larger than those in the other regions. In the study, a method that to add choke blocks in the parallel section along the flow direction in the functional block regions is adopted to increase the flow resistance in local regions and hence to improve flow balance. As shown in

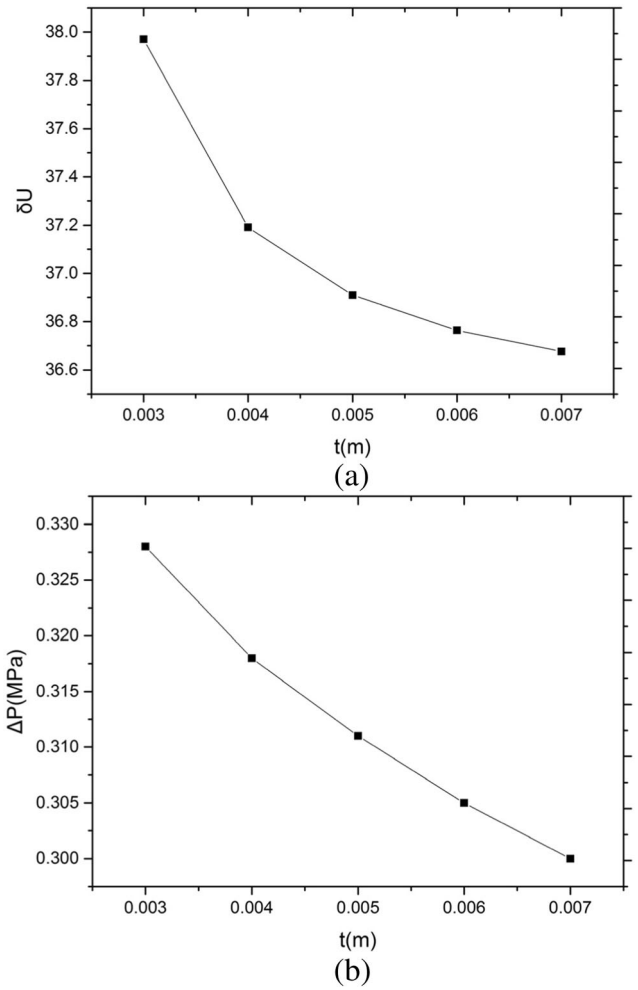

Fig. 11 Variation of flow balance versus different heights of adapter section gap: **a** velocity relative difference δU and **b** maximum pressure drop ΔP

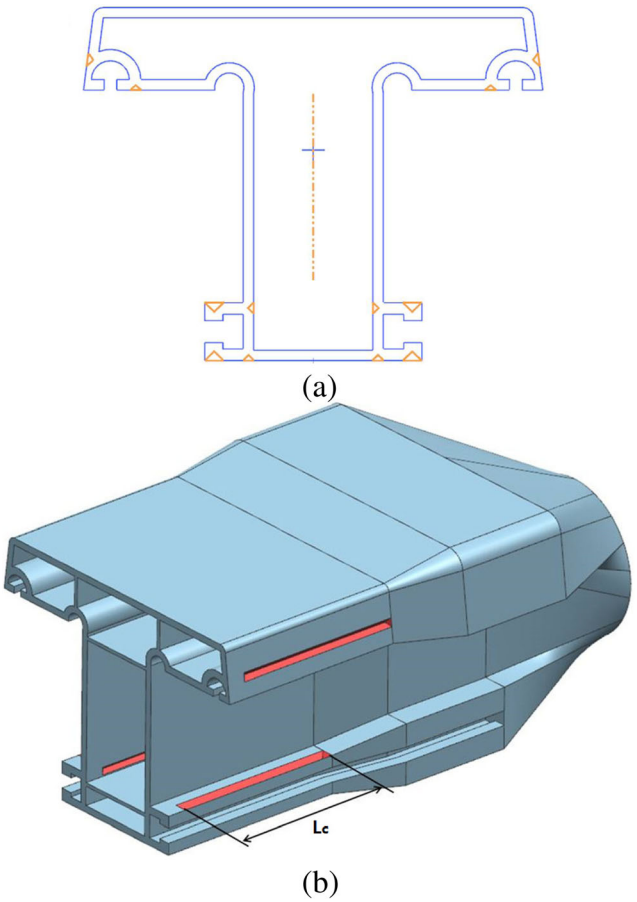

Fig. 12 Geometric parameters of the choke blocks: **a** cross section and **b** longitudinal direction

Fig. 12a, the cross sections of the choke blocks are designed to be triangular and their positions are mainly distributed in the corners and intersections where the flow velocity is found to be obviously larger. The length of the choke block is designed to be $L_c = 0.045$m, which starts from the junction of the parallel section and transition section as shown in Fig. 12b. Figure 13 shows the distribution of axial velocity U_Y at the die exit after the structural adjustment of the die runner. It can be found that the distribution of flow velocity is obviously uniform compared with that before adding the choke blocks, and the velocity gradient is meanwhile reduced in the intersection in functional block regions as shown in Fig. 13b, c, where the flow velocities before and after adding the choke blocks are compared.

Therefore, the adjustment of parallel length and compression ratio in the inner rib regions and the adding of choke blocks in the functional block regions can be an effective method to achieve balanced flow for the die design in complex plastic profile extrusion.

6 Conclusion

The control of flow balance at the die exit for plastic profile is rather difficult because of its complex cross-sectional variation within the die runner. The extrusion die design strategy that considers the different region characteristics of complex plastic profile was proposed in the study, where the inner rib regions were formed through inner flow channel and the mainframe regions were formed through outer flow channel. The numerical method was adopted to investigate the flow behavior of polymer melts within the die runner and hence to verify the feasibility of the die design strategy. The governing equations for three-dimensional polymer melt flow were discretized based on the FVM, and steady pressure-velocity coupling calculation was achieved through the SIMPLE algorithm. According to the numerical results, complex flow behaviors were found in the junction of the transition section and parallel section where the pressure and velocity gradients were relatively large, and much attention should be paid on this region in the die design. The flow velocities in inner rib regions and functional block regions were found to be non-uniform compared with those in the mainframe regions. Based on the analysis of velocity relative difference,

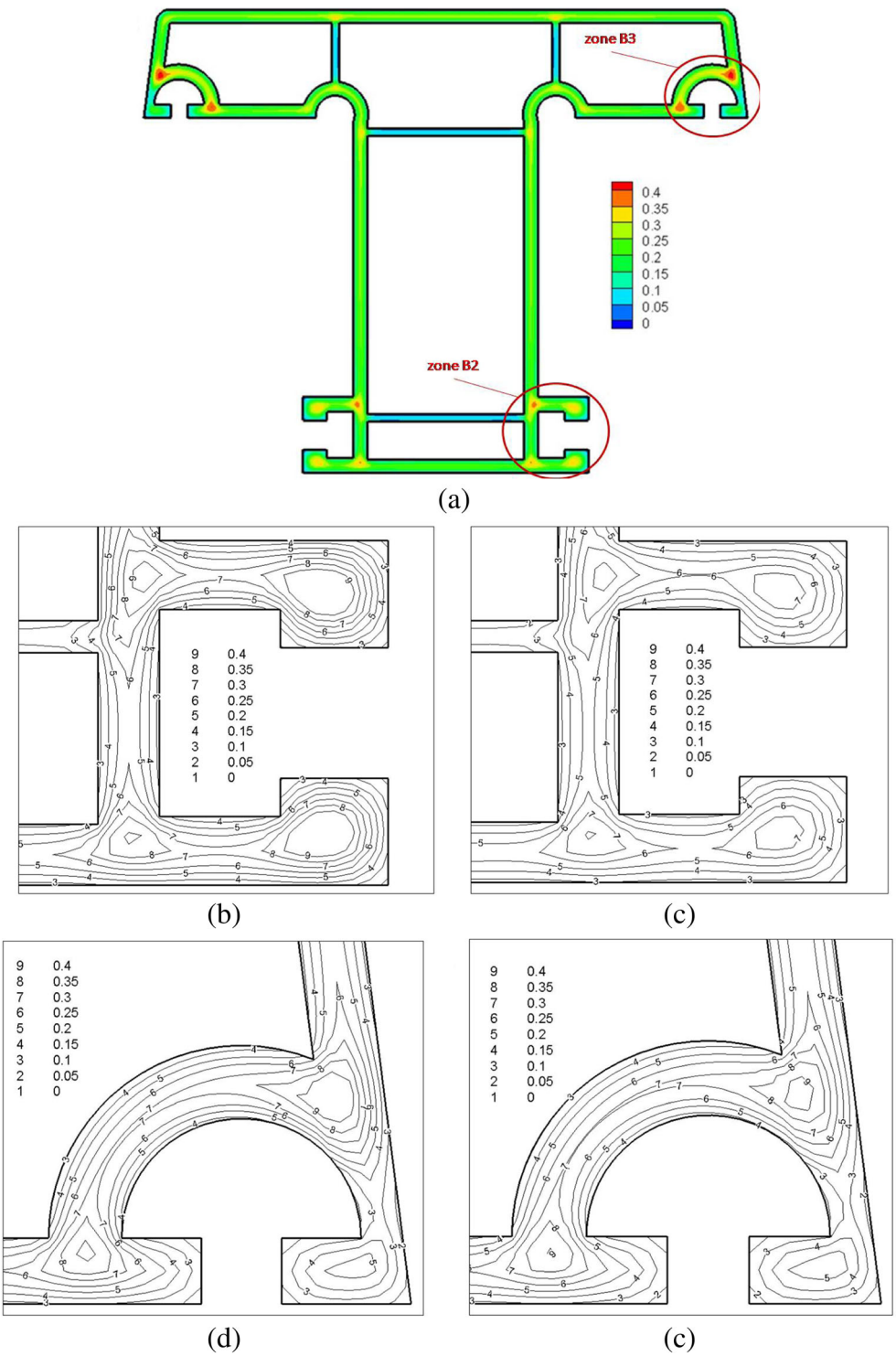

Fig. 13 Contours of axial flow velocity U_Y(m/s): **a** contours of axial flow velocity $U_Y$on the cross section of die lip, **b** contours of axial flow velocity U_Y in functional block region B2 without choke block, **c** contours of axial flow velocity U_Y in functional block region B2 with choke block, **d** contours of axial flow velocity U_Y in functional block region B3 without choke block, and **e** contours of axial flow velocity U_Y in functional block region B3 with choke block

the influence of die geometric structure on flow balance was correspondingly discussed. Through decreasing the parallel length and increasing the compression ratio of inner flow channel in inner rib region, flow balance can be obviously improved. And the adding of the choke blocks can effectively resolve the problem of large velocity difference in the corner and intersection of the functional block regions. Based on the proposed numerical method and die design strategy, further research on how to achieve the optimal die design for complex plastic profile that of significant interest for practical engineering applications will be considered in the future work.

Acknowledgements This work is financially supported by the Natural Science Foundation of China (No. 51675308), the Natural Science

Foundation of China (No. 51205231), and the Natural Science Foundation of Shandong Province (No. ZR2012EEQ001).

References

1. Gonçalves ND, Carneiro OS, Nóbrega JM (2013) Design of complex profile extrusion dies through numerical modeling. J Non-Newton Fluid 200(20):103–110
2. Elgeti S, Probst M, Windeck C, Behr M, Michaeli W (2012) Numerical shape optimization as an approach to extrusion die design. Finite Elem Anal Des 61(6):35–43
3. Mu Y, Zhao GQ, Chen AB, Wu XH (2013) Modeling and simulation of polymer melts flow in the extrusion process of plastic profile with metal insert. Int J Adv Manuf Tech 67(1–4):629–646
4. Mu Y, Zhao GQ, Wu XH, Hang LQ, Chu HH (2015) Continuous modeling and simulation of flow-swell-crystallization behaviors of viscoelastic polymer melts in the hollow profile extrusion process. Appl Math Model 39(3–4):1352–1368
5. Koziey BL, Vlachopoulos J, Vlcek J (1996) Profile die design by pressure balancing and cross flow minimization. Proceedings of SPE Annual Technical Conference: 247–252
6. Hurez P, Tanguy PA, Blouin D (1993) Numerical simulation of profile extrusion dies without flow separation. Polym Eng Sci 33(15):971–979
7. Ettinger HJ, Sienz J, Pittman JFT, Polynkin A (2004) Parameterization and optimization strategies for the automated design of uPVC profile extrusion dies. Struct Multidiscip O 28(10):180–194
8. Mu Y, Zhao GQ, Wu XH, Zhang CR (2010) An optimization strategy for die design in the low-density polyethylene annular extrusion process based on FES/BPNN/NSGA-II. Int J Adv Manuf Tech 50(5):517–532
9. Yilmaz O, Gunes H, Kirkkopru K (2014) Optimization of a profile extrusion die for flow balance. Fiber Polym 15(4):753–761
10. Carneiro OS, Nóbrega JM, Pinho FT, Oliveira PJ (2001) Computer aided rheological design of extrusion dies for profiles. Journal Mater Process Tech 114(1):75–86
11. Švábík J, Plaček L, Sáha P (1999) Profile die design based on flow balancing. Int Polym Process 14(3):247–253
12. Nóbrega JM, Carneiro OS, Oliveira PJ, Pinho FT (2002) Flow balancing in extrusion dies for thermoplastic profiles: part I: automatic design. Int Polym Process 19(3):225–235
13. Carneiro OS, Nóbrega JM (2004) Recent developments in automatic die design for profile extrusion. Plast Rubber Compos 33(33): 400–408
14. Toméa MF, Araujoa MSBD, Alvesb MA, Pinho FT (2008) Numerical simulation of viscoelastic flows using integral constitutive equations: a finite difference approach. J Comput Phys 227(8): 4207–4243
15. Matsuoka T, Takahashi H (1991) Finite element analysis of polymer melt flow in profile extrusion coating die. Int Polym Process 6(3):183–187
16. Kim JM, Kim C, Kim JH, Chung CK, Ahn KH, Lee SJ (2005) High-resolution finite element simulation of 4:1 planar contraction flow of viscoelastic fluid. J Non-Newton Fluid 129:23–37
17. Wachs A, Clermont JR (2000) Non-isothermal viscoelastic flow computations in an axisymmetric contraction at high Weissenberg numbers by a finite volume method. J Non-Newton Fluid 95:147–184
18. Alvesa MA, Pinho FT, Oliveira PJ (2001) The flow of viscoelastic fluids past a cylinder: finite-volume high-resolution methods. J Non-Newton Fluid 97:207–232
19. Beris AN, Dimitropoulos CD (1999) Pseudospectral simulation of turbulent viscoelastic channel flow. Comput Method Appl M 180(3–4):365–392
20. Gao XW (2005) A promising boundary element formulation for three-dimensional viscous flow. Int J Numer Meth Fl 47:19–43
21. Nguyen-Thien T, Tran-Cong T (2000) BEM-neural network approach for polymeric liquids flow analysis. Eng Anal Bound Elem 24:95–106
22. Mu Y, Zhao GQ, Wu XH, Zhai JQ (2013) Finite-element simulation of polymer flow and extrudate swell through hollow profile extrusion die with the multimode differential viscoelastic model. Adv Polym Tech 32:1–19
23. Meijerink JA, van der Vorst HA (1977) An iteration solution method for linear systems of which the coefficient matrix is a symmetric matrix. Math Comput 31(137):148–162
24. van der Vorst HA (1992) Bi-CGSTAB: a fast and smoothly converging variant of Bi-CG for the solution of nonsymmetric linear systems. SIAM J Sci Comput 13(2):631–644
25. Patankar SV, Spalding DB (1972) A calculation procedure for heat, mass and momentum transfer in three-dimensional parabolic flows. Int J Heat Mass Tran 15(10):1787–1806